Digest Journal of Nanomaterials and Biostructures Vol. 10, No. 3, July - September 2015, p. 977 - 984

PREPARATION OF REDUCED GRAPHENE OXIDE/Ag NANOCOMPOSITE FOR PHOTOCATALYTIC HYDROGENATION OF NITROBENZENE TO ANILINE

G. LI*, J. CHANG, C.W. LI
College of Material Science & Engineering, Shenyang Ligong University

In this paper, reduced graphene oxide/silver (RGO-Ag) nanocomposite was synthesized via a simple one-pot hydrothermal method for photocatalytic hydrogenation of nitrobenzene (NB) to aniline. The synthesized nanocomposite was characterized by UV-vis spectroscopy, Raman spectroscopy, FTIR, XPS, TGA and SEM. Results showed that the formation of metallic Ag and reduction of GO was achieved under hydrothermal condition. The result RGO-Ag nanocomposite was used as a novel photocatalyst for hydrogenation of nitrobenzene to aniline under visible light irradiation. Therefore, RGO-Ag nanocomposite can be used as an efficient photocatalyst as an alternative way for organic synthesis. Moreover, a possible mechanism was also proposed to explain the photocatalytic hydrogenation of NB to aniline over the proposed photocatalyst.

(Received June 1, 2015; Accepted August 18, 2015)

Keyword: Ag NPs; SEM; Photocatalysis; XPS;

1. Introduction

Aniline is one of the most important chemicals and intermediates in the production of synthetic dyes, rubber chemicals, amino resins and polyurethane [1, 2]. In general, hydrogenation of nitrobenzene (NB) over a catalyst has been commonly used to produce aniline [3-6]. Traditionally, the synthesis process requires high temperature and high H_2 pressure when using Cu, Ni, Pt, Pd, Au as catalyst [7-10]. In recent years, photocatalytic and electrolytic reduction of nitrobenzene into aniline has been achieved as new techniques [11-14]. Among them, photocatalysis is a promising route for the hydrogenation of nitrobenzene because the production process can be occurred at room temperature and the entire process uses green energy, solar energy, as energy source. Several reports have reported the reduction of NB to aniline by photocatalyst. For example, Wu and co-workers reported photocatalytic hydrogenation of NB to aniline in water over a Bi_2MoO_6 photocatalyst under N_2 atmosphere in the presence of $(NH_4)_2C_2O_4$ as a hole scavenger [15]. Theoretically, the photocatalytic conversion of NB to aniline can be achieved when the conduction band of photocatalyst is lower than ─0.486 V vs. NHE [16].

Recently, graphene, a two-dimensional sp^2-hybridized carbon material, has received considerable attention due to its excellent charge transport mobility, large specific surface area, high electrocatalytic activity and low cost [17-22]. Therefore, it holds great promise for applications in various fields. Reduced graphene oxide (RGO) can be regarded as a narrow-band-gap semiconductor due to the reduction of graphene oxide (GO) partially removes the functional groups on the GO surface [23]. In order to optimize its properties and broaden its application, the addition of nanoparticles (NPs) of inorganic compounds to form a nanocomposite has been studied [24-27]. Among them, silver NPs have been extensively investigated due to its catalytic [28], antibacterial [29], electrical [30], optical [31] and surface-enhanced Raman spectroscopic properties [32, 33]. Therefore, coupling RGO with Ag NPs may result a promising photocatalyst for catalytic hydrogenation of NB to aniline.

By considering the above aspects, the development of RGO-Ag nanocomposite for photocatalytic hydrogenation of nitrobenzene to aniline will be therefore an interesting challenge.

* Corresponding author: gangli_2015@126.com

Herein, we prepared a RGO-Ag nanocomposite via a simple one-pot hydrothermal method. The synthesized nanocomposite was characterized by UV-vis spectroscopy, SEM, TGA, Raman spectroscopy and XPS. We also demonstrate here the excellent photocatalytic activity of the RGO-Ag nanocomposite towards hydrogenation of nitrobenzene to aniline under visible light irradiation.

2. Experimental

2.1 Materials

Synthetic graphite (average particle diameter <20 μm), silver nitrate ($AgNO_3$), ammonium hydroxide (28-30% NH_3 basis), urea and nitrobenzene (NB) were purchased from Sigma-Aldrich. All other chemicals used were analytical grade reagents without further purification. Milli-Q water (18.2 MΩ cm) was used throughout the experiments.

2.2 Preparation of RGO-Ag nanocomposite:

Graphene oxide was prepared using modified Hummer's method [34-37]. In a typical procedure, 125 ml of concentrated sulfuric acid was taken into a flask filled with graphite powder (5 g) followed by the addition of $KMnO_4$ (17.5 g) slowly at 0 °C. The mixture was stirred for 3 h at 35 °C and then diluted by water at 0 °C. After that, H_2O_2 (30 vol.% in water) was added into mixture until the bubbling of the gas was completed. The graphene oxide (GO) powder was collected by centrifugation of the solution and subsequently dried under vacuum at 80°C for 24 h. For preparation of RGO-Ag nanocomposite: GO (10 mg) was added into 120 mL water by 1 h ultrasound under ambient condition, then 5 mL of $AgNO_3$ (20 mM) was added to the dispersion for further 1 h ultrasound. Then, 0.1 g urea was added into above dispersion under stirring. The result suspension was adjusted to pH 9 by ammonia and then transferred to a 50 mL Teflon-lined stainless steel autoclave. The autoclave was heated to 140°C and maintained for 6 h in an oven and naturally cooled down to the room temperature. The final product was obtained after drying in an oven at 70°C for 12 h.

2.3 Characterization

Surface morphology of samples were analyzed by scanning electron microscope (SEM, S-4700, HITACHI). The optical characterizations were obtained by UV-vis spectrophotometer (Specord 2450, Shimadzu). X-ray diffraction patterns were collected from 5° to 80° in 2θ by a XRD with Cu Kα radiation (D8-Advanced, Bruker). Raman analysis was carried out at room temperature using a Raman spectroscope (Renishaw InVia, UK) with a 514 nm laser light. TGA was performed on a Netzsch STA449 C thermogravimetric analyzer from room temperature to 800°C at a heating rate of 10°C/min in N_2 flow. X-ray photoelectron spectroscopy (XPS) spectrum was recorded with PHI 5700 (Physical Electronics, monochromated Al-Kα irradiation, with the binding energy of C^{1s} at 284.8 eV as reference).

2.4 Photocatalytic hydrogenation of nitrobenzene

A 500-W Xenon lamp with an infrared filter and a cut-off filter of 400 nm was used as visible light source. 50 mg of photocatalyst was dispersed in 50 mL of NB-methanol solution (20 mg/L) in a Pyrex reactor. Prior to the catalytic test, the suspension was purged with N_2 to elimination of oxygen. After light illumination, 2 mL of suspension was then taken out a certain period and the photocatalyst was separated by centrifugation. The absorption of NB and aniline was then measured by a UV-vis spectroscopy. The absorbance of NB and aniline at 268 nm and 229 nm was used for measuring the concentration change.

3. Results and discussion

FTIR was adopted for confirming the reduction of GO during the hydrothermal treatment. Figure 1 shows the FTIR spectra of GO and RGO-Ag nanocomposite. As shown from the spectrum of GO, the bands at peaks at 3390, 1730, 1622, 1222, 1050 and 858 cm^{-1}, corresponding to the ─OH stretching, C–O stretching vibrations of the COOH groups, skeletal vibrations of the graphitic domains, C─OH stretching vibrations, C–O stretching and C–O–C stretching, respectively [38]. After the hydrothermal treatment, most of the absorption bands are absent in the spectrum of RGO-Ag nanocomposite except the C−C vibration (1622 cm^{-1}), indicating the removal of oxygen-containing groups on the GO surface.

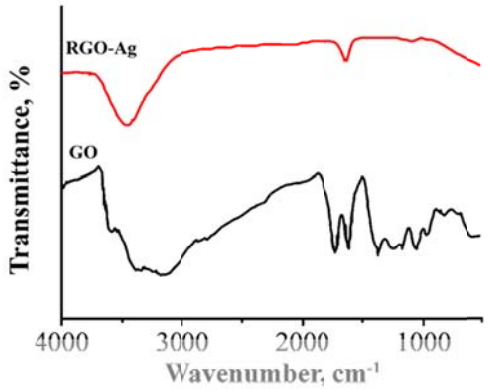

Fig. 1. FTIR spectra of GO and RGO-Ag nanocomposite.

Raman scattering is highly sensitive to the electronic structure change of carbon material, therefore, Raman spectra of graphite, GO and RGO-Ag nanocomposite were then collected. As shown in Figure 2, the spectrum of graphite shows a prominent peak at 1580 cm^{-1}, corresponding to the first-order scattering of the E_{2g}. The spectra of GO and RGO-Ag nanocomposite both exhibit two main characteristic peaks, the D band (approximately 1,340 cm^{-1}) and G band (approximately 1,595 cm^{-1}). The G band represents the plane vibrations with E_{2g} symmetry and is mainly sensitive to the configuration of sp^2 sites, while the D band is related to the breathing mode of κ-point phonon of A_{1g} symmetry [39]. Comparing the intensity ratio of both bands, it can be seen that the increase of I_D/I_G ratio in RGO-Ag nanocomposite compared to that of the GO, suggesting the increase in the average size of the sp^2 sites. According to literatures, it indicates the reduction reaction has taken place [40, 41].

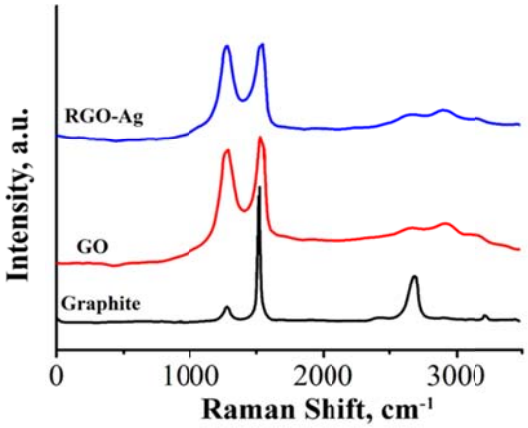

Fig. 2. Raman spectra of graphite, GO and RGO-Ag nanocomposite.

Fig. 3 displays the UV–vis spectra of the dispersions of GO and RGO-Ag nanocomposite. It can be seen that the GO exhibits two characteristic peaks at 231 and 305 nm, corresponding to π-π* transitions of aromatic C—C bonds and n-π* transitions of C=O bonds [42]. After hydrothermal treatment, the absorption peak of GO dispersion at 231 nm red-shifts to 265 nm, and the shoulder absorption peak at 305 nm disappears, further confirming the reduction of GO. Moreover, a new broad absorption peak at 450 nm is observed in the spectrum of RGO-Ag nanocomposite, which could assign to the surface plasmon resonance absorption band of Ag nanoparticles, suggesting the successful formation of Ag NPs [43].

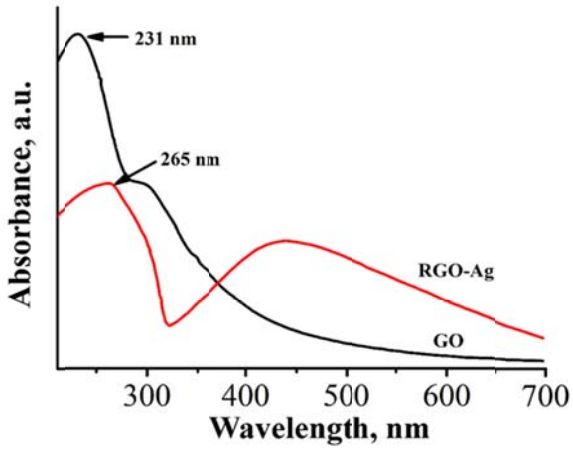

Fig. 3. UV-vis spectra of GO and RGO-Ag nanocomposite.

XPS was used for analyzing the surface chemical composition of RGO-Ag nanocomposite. From Figure 4, we can observe the only existence of C and O in the GO spectrum. However, C, O and Ag peaks are observed in the spectrum of RGO-Ag nanocomposite, indicating the successful formation of RGO-Ag nanocomposite. In high-resolution XPS spectrum (Inset Figure 4), two obvious peaks are observed at 368.3 and 374.4 eV, corresponding to Ag $3d_{5/2}$ and Ag $3d_{3/2}$, respectively [44, 45]. No peaks related to the Ag_2O and AgO are observed during the characterization, indicating the Ag on the RGO sheets are in the metallic form [28]. Therefore, the proposed hydrothermal method could yield high purity of RGO-Ag nanocomposite.

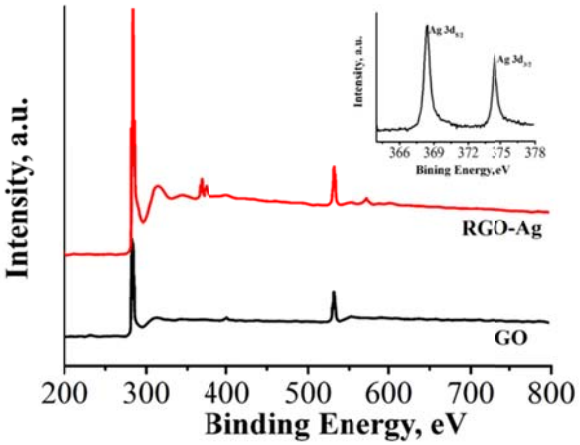

Fig. 4. XPS spectra of GO and RGO-Ag nanocomposite. Inset: high-resolution Ag spectra for RGO-Ag nanocomposite.

The morphology of as-prepared samples were examined by SEM. Figure 5 shows the top-view SEM images of GO and RGO-Ag nanocomposite. Figure 5A shows a typical well dispersed

GO sheets morphology. In comparison with the bare GO sheets, the RGO-Ag nanocomposite exhibits a uniform decoration of Ag NPs between each RGO sheets (Figure 5B). The average particle size of Ag NPs has been calculated as 90 nm (based on more than 200 Ag NPs). As shown in the Figure 4B, the surface decoration of Ag NPs on the RGO sheets could prevent the re-stacking phenomenon of RGO sheets[46]. The result RGO-Ag showed an excellent dispersity, shows no precipitate even over two months.

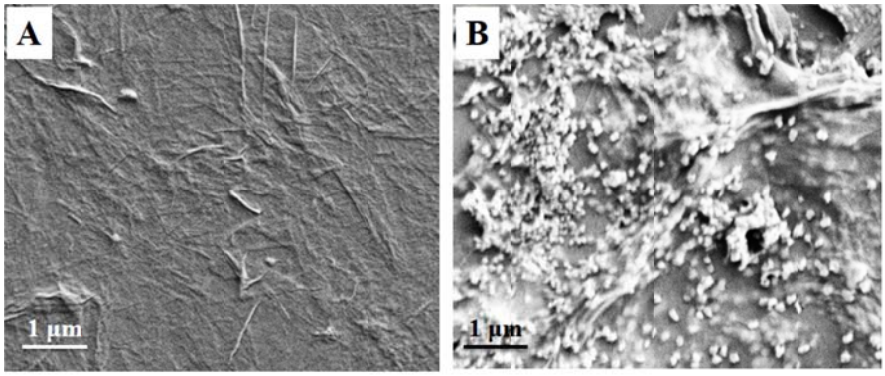

Fig. 5. SEM images of (A) GO and (B) RGO-Ag nanocomposite.

Fig. 6 shows the TGA curves of GO and RGO-Ag nanocomposite. As can be observed, the GO and RGO-Ag exhibit about 4% and 10% weight loss before 120°C due to the evaporation of free H_2O, respectively. Between 110 and 230°C, GO exhibits about 28% weight loss, which can be ascribed to the removal of the oxygen-containing functional groups on its surface [47-49]. However, the RGO-Ag almost has no weight loss in this range, indicating the hydrothermal treatment was already removed most of oxygen containing groups away from GO surface. Comparing with GO, the RGO-Ag nanocomposite shows a restricted weight loss, suggesting that there is a strong interaction between Ag NPs and RGO.

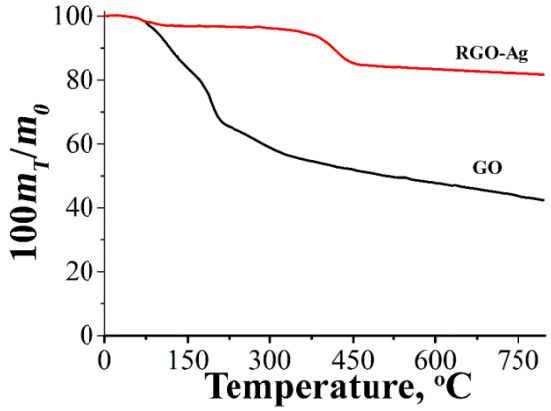

Fig. 6. TGA curves of GO and RGO-Ag from room temperature to 800°C.

Fig. 7A shows the UV-vis spectra of NB solution during the photocatalytic reaction over the RGO-Ag photocatalyst as a function of irradiation time. As shown in the figure, there is a rapid decline in the absorption of NB at 268 nm with increasing of irradiation time. At the sometime, a new peak at 229 nm appears, which corresponds to the absorption of aniline. This suggests that the photocatalytic hydrogenation of NB to aniline could be occurred over the RGO-Ag photocatalyst under visible light irradiation. The conversion profile of using RGO-Ag as photocatalyst for hydrogenation of NB was shown in Figure 7B. It can be seen that there is no conversion process happens without any photocatalyst. However, about 30% of aniline can be detected when using

RGO-Ag nanocomposite as catalyst but without sunlight. In contrast, more than 90% of NB can be converted to aniline after 90 min when the reaction exposes under visible light irradiation. Therefore, our proposed RGO-Ag nanocomposite is a promising candidate of visible-light photocatalyst for hydrogenation of NB to aniline.

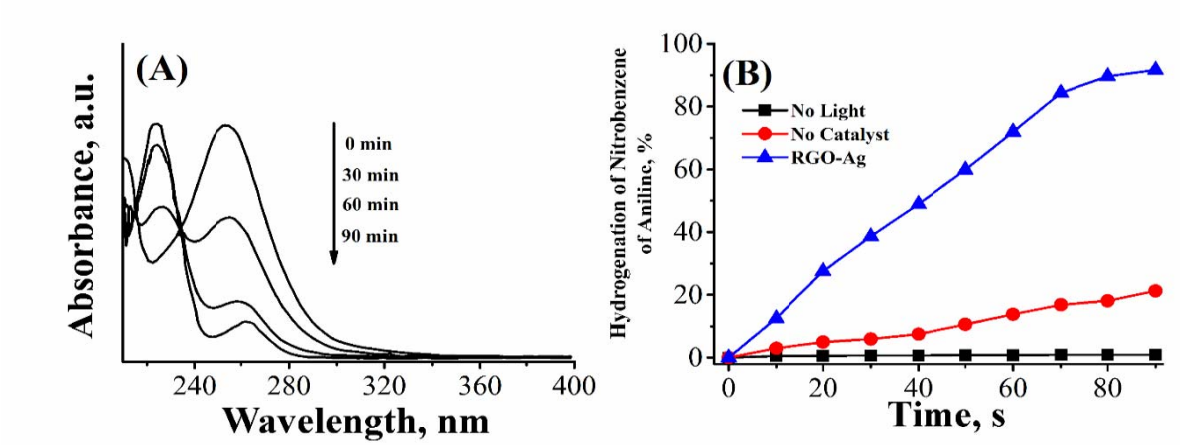

Fig. 7. (A) UV-vis spectra of NB solution monitored during the photocatalytic reaction. (B) Conversion profiles of NB to aniline with no catalyst, no light and RGO-Ag nanocomposite.

The possible mechanism of using RGO-Ag nanocomposite for photocatalytic hydrogenation of NB to aniline can be explained as follow: firstly, the GO could can act as a semiconductor with a large band gap due to the oxygen-containing groups on its basal planes. After hydrothermal treatment, the RGO owing a smaller band gap with higher carrier mobility by removing most of the oxygen-containing groups. A quasi-Fermi level is formed between RGO sheets and Ag NPs. Due to surface plasmon resonance of Ag NPs, electron excitation can happen and electron-hole pairs can formed on the Ag NPs surface when the nanocomposite illuminated by light. Then, due to the excellent electron mobility of RGO, the nanocomposite could effectively suppress the recombination of electron-hole pairs, thus enhance its photocatalytic activity. The reaction can be expressed as follow (Figure 8):

$$Ag \xrightarrow{h\nu} Ag(e^- + h^+)$$

$$CH_3OH + h^+ \longrightarrow CH_3O^\bullet + {}^\bullet CH_2OH$$

$$CH_3O^\bullet + {}^\bullet CH_2OH \longrightarrow 2H^\bullet + 2HCHO$$

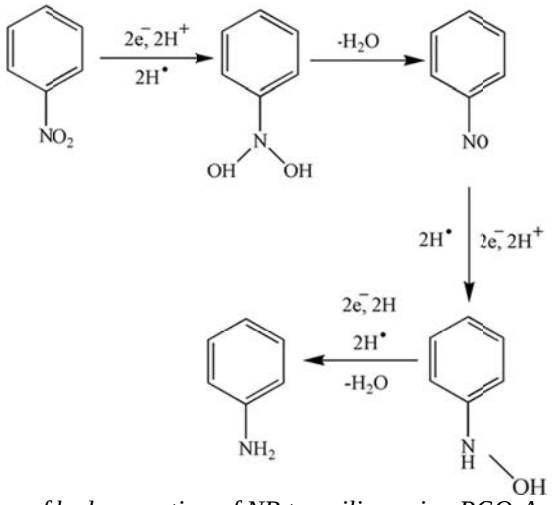

Fig. 8. Mechanism of hydrogenation of NB to aniline using RGO-Ag nanocomposite.

4. Conclusion

In conclusion, we present a one-pot hydrothermal method to synthesize RGO-Ag nanocomposite using GO and $AgNO_3$ as starting materials. The RGO-Ag nanocomposite showed an excellent dispersity with average Ag NPs size of 90 nm. Due to the small band gap and high carrier mobility, the RGO-Ag nanocomposite was used for conversion of NB to aniline by visible light irradiation. The results showed that the RGO-Ag nanocomposite capable to conversion more than 90% of NB within 90 min under experimental conditions.

Reference

[1] E.A. Gelder, S.D. Jackson, C.M. Lok, Chemical Communications **4,** 522 (2005).
[2] S. Diao, W. Qian, G. Luo, F. Wei, Y. Wang, Applied Catalysis A: General **286,** 30 (2005).
[3] M.A. Kohler, J.C. Lee, D.L. Trimm, N.W. Cant, M.S. Wainwright, Applied Catalysis **31,** 309 (1987).
[4] J. Man, Huaxue Fanying Gongcheng Yu Gongyi/Chemical Reaction Engineering and Technology **4,** 64 (1988).
[5] L. Petrov, K. Kumbilieva, N. Kirkov, Applied Catalysis **59,** 31 (1990).
[6] L. Fu, Y. Zheng, Z. Wang, A. Wang, B. Deng, F. Peng, Digest Journal of Nanomaterials and Biostructures **10,** 117 (2015).
[7] A. Corma, P. Concepción, P. Serna, Angewandte Chemie International Edition **46,** 7266 (2007).
[8] J. Wang, Z. Yuan, R. Nie, Z. Hou, X. Zheng, Industrial & Engineering Chemistry Research **49,** 4664 (2010).
[9] S.L. Lee, R. Wickneswari, M.C. Mahani, A.H. Zakri, BIOTROPICA **32,** 213 (2000).
[10] H. Li, Q. Zhao, Y. Wan, W. Dai, M. Qiao, J. Catal. **244,** 251 (2006).
[11] Y. Mu, R.A. Rozendal, K. Rabaey, J. Keller, Environmental Science & Technology **43,** 8690 (2009).
[12] A.-J. Wang, H.-Y. Cheng, B. Liang, N.-Q. Ren, D. Cui, N. Lin, B.H. Kim, K. Rabaey, Environmental Science & Technology **45,** 10186 (2011).
[13] S. Fuldner, P. Pohla, H. Bartling, S. Dankesreiter, R. Stadler, M. Gruber, A. Pfitzner, B. Konig, Green Chemistry **13,** 640 (2011).
[14] Y. Zheng, A. Wang, H. Lin, L. Fu, W. Cai, RSC Advances **5,** 15425 (2015).
[15] W. Wu, R. Lin, L. Shen, R. Liang, R. Yuan, L. Wu, RSC Advances **3,** 10894 (2013).
[16] S. Balasubramanian, Journal of Luminescence **106,** 69 (2004).
[17] K.S. Novoselov, A.K. Geim, S.V. Morozov, D. Jiang, Y. Zhang, S.V. Dubonos, I.V. Grigorieva, A.A. Firsov, Science **306,** 666 (2004).
[18] S. Stankovich, D.A. Dikin, G.H.B. Dommett, K.M. Kohlhaas, E.J. Zimney, E.A. Stach, R.D. Piner, S.T. Nguyen, R.S. Ruoff, Nature **442,** 282 (2006).
[19] A. Wang, L. Fu, H.P. Ng, W. Cai, Y. Zheng, F. Han, Z. Wang, F. Peng, Journal of Non-Oxide Glasses **7,** 1 (2015).
[20] L. He, L. Fu, Y. Tang, Catalysis Science & Technology **5,** 1115 (2015).
[21] L. Fu, T. Xia, Y. Zheng, J. Yang, A. Wang, Z. Wang, Ceram Int **41,** 5903 (2015).
[22] A. Wang, H.P. Ng, Y. Xu, Y. Li, Y. Zheng, J. Yu, F. Han, F. Peng, L. Fu, Journal of Nanomaterials **2014,** 6 (2014).
[23] A.H. Qusti, R.M. Mohamed, M. Abdel Salam, Ceram Int **40,** 5539 (2014).
[24] A.K. Geim, K.S. Novoselov, Nature Materials **6,** 183 (2007).
[25] F. Schedin, A.K. Geim, S.V. Morozov, E.W. Hill, P. Blake, M.I. Katsnelson, K.S. Novoselov, Nat Mater **6,** 652 (2007).

[26] L. Fu, Y. Zheng, A. Wang, W. Cai, H. Lin, Food Chemistry **181,** 127 (2015).
[27] L. Fu, A. Wang, Y. Zheng, W. Cai, Z. Fu, Materials Letters **142,** 119 (2015).
[28] R. Liu, S. Li, X. Yu, G. Zhang, Y. Ma, J. Yao, Journal of Materials Chemistry **21,** 14917 (2011).
[29] J. Shen, M. Shi, N. Li, B. Yan, H. Ma, Y. Hu, M. Ye, Nano Research **3,** 339 (2010).
[30] G. Li, T. Wang, Y. Zhu, S. Zhang, C. Mao, J. Wu, B. Jin, Y. Tian, Appl Surf Sci **257,** 6568 (2011).
[31] A. Slistan-Grijalva, R. Herrera-Urbina, J.F. Rivas-Silva, M. Ávalos-Borja, F.F. Castillón-Barraza, A. Posada-Amarillas, Mater Res Bull **43,** 90 (2008).
[32] Z. Zhang, F. Xu, W. Yang, M. Guo, X. Wang, B. Zhang, J. Tang, Chemical Communications **47,** 6440 (2011).
[33] L. Fu, Y. Zheng, Q. Ren, A. Wang, B. Deng, Journal of Ovonic Research **11,** 21 (2015).
[34] S. Park, J. An, R.D. Piner, I. Jung, D. Yang, A. Velamakanni, S.T. Nguyen, R.S. Ruoff, Chemistry of Materials **20,** 6592 (2008).
[35] W.S. Hummers, R.E. Offeman, Journal of the American Chemical Society **80,** 1339 (1958).
[36] L. Fu, Z. Fu, Ceram Int **41,** 2492 (2015).
[37] L. Fu, W. Cai, A. Wang, Y. Zheng, Materials Letters **142,** 201 (2015).
[38] J. Xu, K. Wang, S.-Z. Zu, B.-H. Han, Z. Wei, ACS Nano **4,** 5019 (2010).
[39] D. Yang, A. Velamakanni, G. Bozoklu, S. Park, M. Stoller, R.D. Piner, S. Stankovich, I. Jung, D.A. Field, C.A. Ventrice Jr, R.S. Ruoff, Carbon **47,** 145 (2009).
[40] X. Li, Q. Wang, Y. Zhao, W. Wu, J. Chen, H. Meng, Journal of colloid and interface science **411,** 69 (2013).
[41] H.N. Tien, V.H. Luan, L.T. Hoa, N.T. Khoa, S.H. Hahn, J.S. Chung, E.W. Shin, S.H. Hur, Chemical Engineering Journal **229,** 126 (2013).
[42] J.I. Paredes, S. Villar-Rodil, A. Martínez-Alonso, J.M.D. Tascón, Langmuir **24,** 10560 (2008).
[43] W. Yuan, Y. Gu, L. Li, Appl Surf Sci **261,** 753 (2012).
[44] A.I. Lukman, B. Gong, C.E. Marjo, U. Roessner, A.T. Harris, Journal of colloid and interface science **353,** 433 (2011).
[45] C. Tian, Q. Zhang, B. Jiang, G. Tian, H. Fu, J Alloy Compd **509,** 6935 (2011).
[46] B. Li, T. Liu, Y. Wang, Z. Wang, Journal of colloid and interface science **377,** 114 (2012).
[47] C. Zhu, S. Guo, Y. Fang, S. Dong, ACS Nano **4,** 2429 (2010).
[48] A. Lerf, H. He, M. Forster, J. Klinowski, J Phys Chem B **102,** 4477 (1998).
[49] G. Wang, Z. Yang, X. Li, C. Li, Carbon **43,** 2564 (2005).